

DECONVOLUTION OF PLENACOUSTIC IMAGES

Lucio Bianchi, Dejan Marković, Fabio Antonacci, Augusto Sarti, Stefano Tubaro

Dipartimento di Elettronica, Informazione e Bioingegneria, Politecnico di Milano
Piazza Leonardo da Vinci 32 – 20133 Milano, Italy

ABSTRACT

In this paper we propose a methodology aimed at improving the resolution capabilities of plenacoustic imaging, which is based on deconvolution techniques mutated from aerospace acoustic imaging. In order to reduce the computational burden, we also propose a modification of the minimization problem that exploits the highly structured information contained in the plenacoustic image. Experiments and simulations show the improvement of the accuracy gained by applying the deconvolution operator.

Index Terms— Plenacoustic imaging, acoustic imaging, deconvolution, microphone array.

1. INTRODUCTION

Acoustic scene analysis aims at retrieving geometric and radiative properties of acoustic sources and reflectors, and many applications could benefit from the gathered knowledge. A relevant example is sound field rendering [1].

Recently, in [2] authors have addressed the problem of acoustic scene analysis through plenacoustic imaging, which consists in retrieving the distribution of energy of acoustic rays that impinge on a microphone array. In particular, the array is conceived as an observation window of the sound field. Using tools of image pattern analysis, authors tackle different problems of acoustic scene analysis, such as source and reflector localization. The advantage of plenacoustic imaging is that several problems can be solved using the same data, without resorting to ad-hoc representations suitable for the specific problem at hand.

In [2] the array of M microphones is subdivided into sub-arrays, composed by W adjacent sensors each. For each sub-array the pseudospectrum is computed through Minimum Variance Distortionless Response (MVDR) beamforming [3]. In the geometrical acoustics representation, the pseudospectrum can be seen as an estimate of the distribution of the energy of rays passing through the center of the sub-array. The plenacoustic image is then approximated by the juxtaposition of the different pseudospectra. As the number of sensors in each sub-array decreases, the resolution of pseudospectra decreases as well. On the other hand, by decreasing the number of sensors in each sub-array, a higher number of pseudospectra composes the plenacoustic image. A trade-off issue, therefore, arises. This trade-off has important consequences on applications. Let us consider, for example, the task of source localization. A point-like acoustic source is mapped on the plenacoustic image as a line, and the estimate of the location is accomplished by finding linear patterns. By decreasing W , location of the peaks becomes undetermined due to the poor resolution of the acoustic images, but more data are available, as the plenacoustic image is composed by a higher number of pseudospectra.

We aim at overcoming this trade-off issue using deconvolution techniques mutated from research in aerospace acoustic imaging. Let us consider, for the moment, the presence of a single point-like source, and a microphone array with an arbitrary extension and infinite number of sensors. Pseudospectra of the sub-arrays appear as Dirac deltas in the direction of the acoustic source. In a real scenario (i.e. finite number of sensors), however, a smearing of the pseudospectrum appears. Such smearing can be modeled by the Point Spread Function (PSF) [4], which depends on the position of the source and of the sensors in the array. There are several techniques in the literature for deconvolution of PSF. Relevant examples are [5, 6]. In this paper we apply the deconvolution operator for improving the resolution of plenacoustic imaging. Moreover, in order to reduce the computational cost, we propose a two-step modification of the deconvolution algorithm that exploits the information contained in the plenacoustic image. The original plenacoustic image is first analysed to gather as much information as possible about the location of active sources. This information is then used to speed up the deconvolution.

We show the advantages of the proposed technique with two relevant examples. First, we show that deconvolution enables the acquisition of accurate plenacoustic images also for extended sources. A second example proves, by means of simulations and experiments, that deconvolution enables the localization of multiple acoustic sources even when they are in unfavourable locations with respect to the microphone array.

The rest of the paper is organized as follows: section 2 introduces the notation. Section 3 models the plenacoustic image, formulates the problem, and provides the theoretical support for the deconvolution, investigated in section 4. Section 5 discusses some examples that show the advantages of deconvolution. Finally, section 6 draws some conclusive remarks.

2. NOTATION

In this section we introduce the notation used throughout the rest of the paper. Consider the setup in Fig. 1. L acoustic sources are located in $\mathbf{p}_{S,l} = [x_{S,l} \ y_{S,l}]^T$ and produce wideband signals $s_l(t)$, $l = 1, \dots, L$. An uniform linear array of M microphones is placed on the y axis between $y = -q_0$ and $y = +q_0$. The i th microphone is at $\mathbf{m}_i = [0 \ q_0 - 2q_0(i-1)/(M-1)]^T$, $i = 1, \dots, M$. We divide the array into $M - W + 1$ sub-arrays, where W is the (odd) number of microphones in each sub-array. Microphones belonging to the sub-array centered in \mathbf{m}_i are denoted by \mathbf{m}_j , $j = i - (W-1)/2, \dots, i + (W-1)/2$, and they acquire the signals $x_j(t)$. The signal $x_j(t)$ is processed with a filter bank to obtain $x_j(t, \omega_k)$, $k = 1, \dots, K$, ω_k being the central frequency of the k th sub-band. These signals are then stacked into the vector $\mathbf{x}_i(t, \omega_k) = [x_{i-(W-1)/2}(t, \omega_k) \ \dots \ x_{i+(W-1)/2}(t, \omega_k)]^T$.

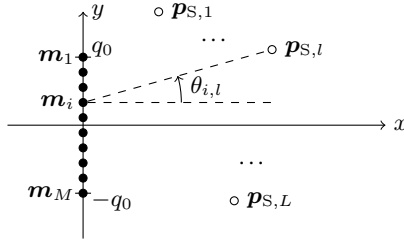


Figure 1: Geometric setup of the microphone array and acoustic sources.

We can express $\mathbf{x}_i(t, \omega_k)$ as [3]

$$\mathbf{x}_i(t, \omega_k) = \mathbf{A}_i(\omega_k)\mathbf{S}(t, \omega_k) + \mathbf{v}(t, \omega_k), \quad (1)$$

where $\mathbf{S}(t, \omega_k) = [s_1(t, \omega_k) \ \dots \ s_L(t, \omega_k)]^T$ contains the source signals and $\mathbf{v}(t, \omega_k)$ is a zero-mean additive noise with covariance matrix $\sigma^2\mathbf{I}$, \mathbf{I} being the identity matrix of dimensions $W \times W$. $\mathbf{A}_i(\omega_k)$ is the collection of steering vectors towards each of the L sources in the k th frequency sub-band, i.e.

$$\mathbf{A}_i(\omega_k) = [\mathbf{a}(\theta_{i,1}, \omega_k) \ \dots \ \mathbf{a}(\theta_{i,L}, \omega_k)]. \quad (2)$$

The symbol $\theta_{i,l}$ denotes the angle under which the l th source is seen from the microphone at \mathbf{m}_i . With reference to Fig. 1, we have

$$\theta_{i,l} = \arctan\left(\frac{y_{S,l} - q_0 + 2q_0(i-1)/(M-1)}{x_{S,l}}\right). \quad (3)$$

3. DATA MODEL

In [2], the goal is to estimate the power associated to acoustic rays that intersect the microphone array. Authors approximate plenacoustic images through beamforming on the signals acquired by sub-arrays. In particular, pseudospectra computed by individual sub-arrays are represented in the ray space \mathcal{P} . According to [2], a ray is the set of points (x, y) that satisfy $y = mx + q$. The pair of parameters (m, q) uniquely identifies a ray and defines the ray space \mathcal{P} . Acoustic primitives are represented in \mathcal{P} as the set of rays that pass through them. In particular, sources and reflectors become in \mathcal{P} lines and wedge-shaped regions, respectively. For further details we invite the interested reader to [7], where this representation was first adopted.

With reference to the notation introduced in Sec. 2, a suitable beamforming technique computes the pseudospectrum $p_i(\theta, \omega_k)$ for the sub-array centered in \mathbf{m}_i [2, 3], which can be considered as the estimate of the energy of acoustic rays insiding on the central microphone at \mathbf{m}_i . Pseudospectra $p_i(\theta, \omega_k)$ are then converted to $p_i(m, q, \omega_k)$, whose domain is \mathcal{P} , through

$$\begin{aligned} m &= \tan(\theta), \\ q &= q_0 - 2q_0(i-1)/(M-1). \end{aligned} \quad (4)$$

The plenacoustic image $\mathcal{I}(m, q, \omega_k)$ is, finally, the juxtaposition of $p_i(m, q, \omega_k)$, i.e.

$$\mathcal{I}(m, q_i, \omega_k) = p_i(m, q, \omega_k), \quad (5)$$

where $q = q_i = q_0 - 2q_0(i-1)/(M-1)$. In [2] authors also propose a wideband version of plenacoustic imaging by averaging

pseudospectra in a frequency sub-band fashion. In the following, we specify if we are working either in narrowband or wideband. For compactness, however, we drop the dependency on ω_k .

No matter what beamforming technique is used to extract $p_i(\theta)$, pseudospectra depend on the covariance matrix \mathbf{R}_i of the signals acquired by the sensors in the i th sub-array. It is known in the literature [3] that

$$\mathbf{R}_i = \mathbb{E}\{\mathbf{x}_i(t)\mathbf{x}_i(t)^H\} = \mathbf{A}_i\mathbf{D}\mathbf{A}_i^H + \sigma^2\mathbf{I}, \quad (6)$$

where \mathbf{D} is the covariance matrix of the L sources. For L uncorrelated sources with variance σ_l^2 we have

$$\mathbf{D} = \text{diag}([\sigma_1^2 \ \dots \ \sigma_L^2]). \quad (7)$$

Let us denote with $\mathbf{h}_i(\theta)$ the spatial filter that performs the beamforming on the i th sub-array towards direction θ . Different techniques could be used, such as Minimum Variance Distortionless Beamformer (MVDR) or Delay and Sum (DAS) [3]. No matter what technique is used, the pseudospectrum is obtained as

$$p_i(\theta) = \mathbf{h}_i(\theta)^H \mathbf{R}_i \mathbf{h}_i(\theta). \quad (8)$$

For the DAS beamformer $\mathbf{h}_i(\theta) = \mathbf{a}(\theta)/W$ and

$$p_i(\theta) = \frac{1}{W^2} [\mathbf{a}(\theta)^H \mathbf{A}_i \mathbf{D} \mathbf{A}_i^H \mathbf{a}(\theta) + \sigma^2 \mathbf{a}(\theta)^H \mathbf{a}(\theta)]. \quad (9)$$

In ideal conditions (i.e. infinite number of microphones) the first addend on the right-hand side is equal to zero for angles $\theta \neq \theta_{i,l}$ and equal to σ_l^2 for $\theta = \theta_{i,l}$. For sub-arrays with a finite resolution, however, the pseudospectrum takes a non-zero value also for angles $\theta \neq \theta_{i,l}$. This effect is modeled in the literature through the Point Spread Function (PSF) [4]. These considerations can be applied also to beamforming techniques different from DAS. In the next section we summarize a methodology, originally proposed in [6], which attenuates the effect of the PSF through a deconvolution operation.

4. DECONVOLUTION

In this section we review the Covariance Matrix Fitting methodology, originally presented in [6], for the estimation of sources location and power. This methodology is based on the computation of the sample covariance matrix

$$\hat{\mathbf{R}}_i = \frac{1}{T} \sum_{t=1}^T \mathbf{x}_i(t)\mathbf{x}_i(t)^H. \quad (10)$$

It is worth noticing that the number L of sources is unknown in practical applications. As a consequence, we perform a grid search. Let N be the number of possible directions of arrival of the source. We accordingly modify the steering vectors, which now are computed on the grid of angles $\theta_{i,n}$, $n = 1, \dots, N$. Associated to the directions $\theta_{i,n}$ are the signals power σ_n^2 . The matrix \mathbf{D} , introduced in (7), now generalizes to $\mathbf{D} = \text{diag}([\sigma_1^2 \ \dots \ \sigma_N^2])$. Under the assumption that $N \gg L$, we can model \mathbf{D} as sparse. The signal powers σ_n^2 and the additive noise power σ^2 are therefore estimated by solving the quadratic convex optimization problem [8]

$$\begin{aligned} &\underset{\sigma_n^2, n=1, \dots, N, \sigma^2}{\text{minimize}} && \|\hat{\mathbf{R}}_i - \mathbf{A}_i \mathbf{D} \mathbf{A}_i^H - \sigma^2 \mathbf{I}\|_F^2 \\ &\text{subject to} && \sigma_n^2 \geq 0, \ n = 1, \dots, N, \\ &&& \sum_{n=1}^N \sigma_n^2 \leq \lambda_i, \ \sigma^2 \geq 0, \end{aligned} \quad (11)$$

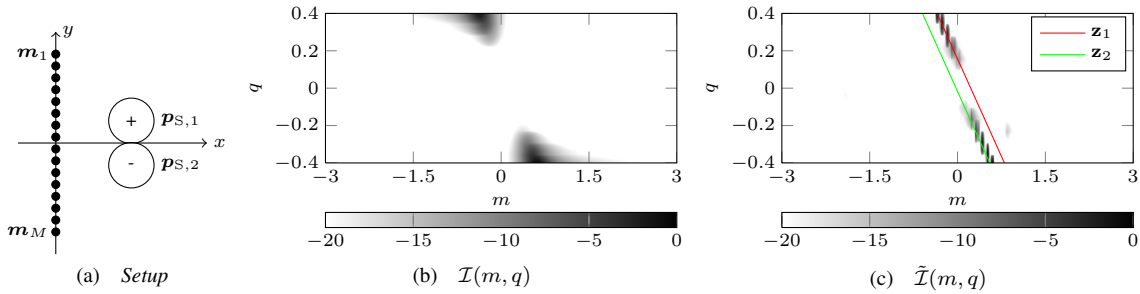


Figure 2: Comparison between non-deconvolved (Fig. 2b) and deconvolved (Fig. 2c) plenacoustic images for the setup in Fig. 2a. Grayscale plenacoustic images are represented in dB scale between 0 dB and -20 dB.

where $\|\cdot\|_F$ denotes the Frobenius norm. Let $\hat{\mathbf{R}}_i = \hat{\mathbf{U}}_i \hat{\mathbf{\Gamma}}_i \hat{\mathbf{U}}_i^H$ be the eigendecomposition of $\hat{\mathbf{R}}_i$. The parameter λ_i is given by

$$\lambda_i = \text{Tr}(\hat{\mathbf{\Gamma}}_i - \hat{\gamma}_i \mathbf{I}), \quad (12)$$

$\hat{\gamma}_i$ being the smallest eigenvalue of $\hat{\mathbf{R}}_i$. The number of unknowns in (11) is $N + 1$.

The problem formulation in (11) assumes the signal sources to be uncorrelated. In real acoustic scenes, however, we cannot consider sources as point-like, especially in near-field. Consequently, there is a set of directions $\theta_{i,n}$ from which correlated signals impinge on the i th sub-array. In [6] an extension to correlated sources is proposed. The matrix \mathbf{D} is not diagonal any more, and the optimization problem can be reformulated as the semi-definite quadratic program [8]

$$\begin{aligned} & \underset{\sigma^2, \mathbf{D}}{\text{minimize}} && \|\hat{\mathbf{R}}_i - \mathbf{A}_i \mathbf{D} \mathbf{A}_i^H - \sigma^2 \mathbf{I}\|_F^2 \\ & \text{subject to} && \mathbf{D} \geq 0, \text{Tr}(\mathbf{D}) \leq \lambda_i, \sigma^2 \geq 0. \end{aligned} \quad (13)$$

The number of unknowns is now $N^2 + 1$, therefore the solution of the problem requires a high computational cost. The increase in the computational cost becomes evident if we consider the case of wideband sources, as the minimization must be accomplished K times.

As shown in [2], it is possible to estimate the number of sources \hat{L} along with their position $\hat{\mathbf{p}}_{S,l}$ through pattern analysis on the plenacoustic image. We take advantage of this information to reduce the computational burden of the deconvolution. More specifically, we replace the number of scanning directions N with the number of sources \hat{L} estimated from a preliminary analysis of the non-deconvolved plenacoustic image, and consider the steering matrix

$$\mathbf{A}_i = \left[\mathbf{a}(\hat{\theta}_{i,1}) \quad \dots \quad \mathbf{a}(\hat{\theta}_{i,\hat{L}}) \right]. \quad (14)$$

The symbol $\hat{\theta}_{i,l}$ denotes the angle under which a source in $\hat{\mathbf{p}}_{S,l}$ is seen from the microphone in \mathbf{m}_i . Thanks to this substitution, the number of unknowns in problems (11) and (13) reduces to $\hat{L} + 1$ and $\hat{L}^2 + 1$, respectively. However, the sparsity of the problem is not guaranteed any more. Moreover, an erroneous estimate $\hat{\mathbf{p}}_{S,l}$ could lead to wrong results. For the above reasons, we do not consider only sources in $\hat{\mathbf{p}}_{S,l}$, but also in their neighbourhood, i.e. we perform the deconvolution on the grid of $\hat{\mathbf{p}}_{S,l}$,

$$\begin{aligned} \hat{\mathbf{p}}_{S,l} \in \{ \mathbf{p}_{S,l} : \mathbf{p}_{S,l} = \hat{\mathbf{p}}_{S,l} + \boldsymbol{\delta}, \boldsymbol{\delta} = [\delta_x \quad \delta_y]^T, \\ -\delta_{\max} \leq \delta_x, \delta_y \leq \delta_{\max} \}. \end{aligned} \quad (15)$$

The steering vectors become

$$\mathbf{A}_i = \left[\mathbf{a}(\hat{\theta}_{i,1}) \quad \dots \quad \mathbf{a}(\hat{\theta}_{i,\hat{L}}) \right], \quad (16)$$

where $\hat{\theta}_{i,l}$ are the directions associated to $\hat{\mathbf{p}}_{S,l}$ from the i th sub-array. The optimization problem is now sparse and is more robust against possible errors in the preliminary analysis. Finally, the deconvolved pseudospectra are

$$\tilde{p}_i(\theta_{i,n}) = \{\mathbf{D}\}_n^n, \quad (17)$$

where $\{\mathbf{D}\}_n^n$ denotes the n th entry on the diagonal of \mathbf{D} . The deconvolved plenacoustic image $\tilde{\mathcal{I}}(m, q)$ becomes the juxtaposition of $\tilde{p}_{i,k}(m, q)$, similarly to (5). If we are interested in the extension to wideband signals, we can proceed as in [9] by averaging pseudospectra in a frequency sub-band fashion.

5. RESULTS

In this section we present simulations and experimental results to prove the advantages of deconvolution in plenacoustic imaging. We consider an uniform linear array of length 0.9 m ($q_0 = 0.45$ m) composed by $M = 16$ microphones. The array is divided into 14 sub-arrays, with $W = 3$. For all the simulations and the experiments, we consider the signals acquired by the microphones to be affected by an additive noise, whose power determines a Signal-to-Noise Ratio equal to 10 dB. Non-deconvolved pseudospectra are obtained with MVDR beamformer, while deconvolved pseudospectra are obtained by solving the optimization problems in (11) or (13) with the CVX Matlab[®] toolbox [10].

5.1. Extended Source

Consider the acoustic scene depicted in Fig. 2a. The acoustic source consists in two discs of radii $r = 0.08$ m and their centers are placed at $\mathbf{p}_{S,1} = [0.6 \text{ m} \quad 0.08 \text{ m}]^T$ and $\mathbf{p}_{S,2} = [0.6 \text{ m} \quad -0.08 \text{ m}]^T$. The signals emitted by the two discs are opposite in sign. We simulated such setup with the k-Wave toolbox [11]. We expect the plenacoustic image to exhibit two parallel lines \mathbf{z}_1 and \mathbf{z}_2 , corresponding to the centers of the discs $\mathbf{p}_{S,1}$ and $\mathbf{p}_{S,2}$, respectively. Moreover, we expect the disc in $\mathbf{p}_{S,1}$ to be occluded by the one in $\mathbf{p}_{S,2}$ for sub-arrays in the half-space $y < 0$, and viceversa for sub-arrays in the half-space $y > 0$. Finally, due to the mutual cancellation of contributions from the two discs, the image should exhibit a null region for sub-arrays close to the origin. Fig. 2b and

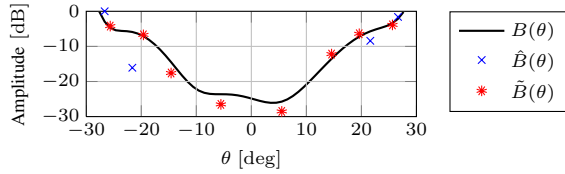


Figure 3: Comparison of radiation patterns estimated from $\mathcal{I}(m, q)$ and $\tilde{\mathcal{I}}(m, q)$.

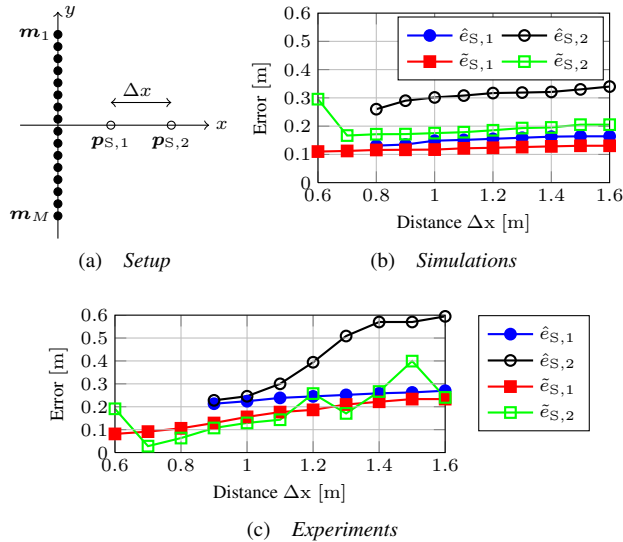


Figure 4: Average localization error for the setup in Fig. 4a. Simulations (Fig. 4b) and experiments (Fig. 4c)

Fig. 2c show the plenacoustic images $\mathcal{I}(m, q)$ and $\tilde{\mathcal{I}}(m, q)$, respectively, at $f = 1$ kHz. The non-deconvolved plenacoustic image $\mathcal{I}(m, q)$ suffers from a smearing of the peaks and does not present significant energy in the range $-0.2 \leq q \leq 0.2$. On the other hand, the deconvolved plenacoustic image is composed by two parallel lines. The increase of definition gained with the deconvolution enables further analysis on the plenacoustic image. As an example, Fig. 3 shows the actual radiation pattern $B(\theta)$ of the source. $B(\theta)$ has been estimated by placing in the simulation setup 360 microphones around the source. Fig. 3 also shows the patterns $\hat{B}(\theta)$ and $\tilde{B}(\theta)$ estimated from $\mathcal{I}(m, q)$ and $\tilde{\mathcal{I}}(m, q)$, respectively. Note that $\hat{B}(\theta)$ takes values only at very few points, due to the absence of relevant peaks in the non-deconvolved pseudospectra in $\mathcal{I}(m, q)$. On the other hand, $\tilde{B}(\theta)$ closely approximates $B(\theta)$ for a significant number of points, thanks to the higher resolution of $\tilde{\mathcal{I}}(m, q)$.

5.2. Localization

Consider the setup depicted in Fig. 4a. Two point-like sources are located in $\mathbf{p}_{S,1} = [1 \text{ m} \ 0 \text{ m}]$, and $\mathbf{p}_{S,2} = [(1 + \Delta x) \text{ m} \ 0 \text{ m}]$, where Δx is in the range (0.6 m, 1.6 m). Localization is performed through suitable image pattern analysis on the plenacoustic images $\mathcal{I}(m, q)$ and $\tilde{\mathcal{I}}(m, q)$, as in [2]. We denote the errors on $\mathbf{p}_{S,1}$ and $\mathbf{p}_{S,2}$ from $\mathcal{I}(m, q)$ as $\hat{e}_{S,1}$ and $\hat{e}_{S,2}$, respectively, while $\tilde{e}_{S,1}$ and $\tilde{e}_{S,2}$ are the localization errors from $\tilde{\mathcal{I}}(m, q)$. One hundred indepen-

dent realizations of the simulations are performed for each location $\mathbf{p}_{S,2}$. Fig. 4b shows the average value of the localization errors as a function of the distance Δx . Notice that the deconvolution enables to accurately localize both sources in $\mathbf{p}_{S,1}$ and $\mathbf{p}_{S,2}$ starting from $\Delta x = 0.7$ m, while without the deconvolution the localization is possible only from $\Delta x = 0.8$ m.

Fig. 4c shows the average localization error for ten realizations of an experiment that reproduces the setup in Fig. 4a. Sources and microphones have been deployed in a modestly reverberant room. Notice that the localization error exhibits a trend similar to Fig. 4b, thus confirming the validity of the proposed technique also in real-world conditions. Moreover, with real-world data, the error $\hat{e}_{S,2}$ increases with Δx , while $\tilde{e}_{S,2}$ is almost constant.

6. CONCLUSIONS

In this work we have proposed a methodology for the deconvolution of plenacoustic images aimed at improving the resolution capabilities. Deconvolution is based on the Covariance Matrix Fitting technique. In order to reduce the computational cost, we also propose a modification of the algorithm, which takes advantage of the information contained in the plenacoustic image. By applying the deconvolution novel applications of plenacoustic imaging are possible, such as the estimation of the radiance pattern of acoustic sources.

7. REFERENCES

- [1] T. Betlehem and T. Abhayapala, "Theory and design of soundfield reproduction in reverberant rooms," *J. Acoust. Soc. Am.*, vol. 117, no. 4, pp. 2100–2111, 2005.
- [2] D. Marković, F. Antonacci, A. Sarti, and S. Tubaro, "Soundfield imaging in the ray space," *IEEE Trans. Audio, Speech, Lang. Process.*, 2013, doi: 10.1109/TASL.2013.2274697.
- [3] P. Stoica and R. Moses, *Spectral Analysis of Signals*. Upper Saddle River, New Jersey: Prentice Hall, 2005.
- [4] F. Ribeiro and V. Nascimento, "Fast transforms for acoustic imaging - Part I: Theory," *IEEE Trans. Image Process.*, vol. 20, no. 8, pp. 2229–2240, 2011.
- [5] T. Brooks and W. Humphreys, "A deconvolution approach for the mapping of acoustics sources (DAMAS) determined from phased microphone arrays," *Journal of Sound and Vibration*, vol. 294, pp. 856–879, 2006.
- [6] T. Yardibi, J. Li, P. Stoica, and L. Cattafesta III, "Sparsity constrained deconvolution approaches for acoustic source mapping," *J. Acoust. Soc. Am.*, vol. 123, no. 5, pp. 2631–2642, 2008.
- [7] F. Antonacci, M. Foco, A. Sarti, and S. Tubaro, "Fast tracing of acoustic beams and paths through visibility lookup," *IEEE Trans. Audio, Speech, Lang. Process.*, vol. 16, no. 4, pp. 812–824, 2008.
- [8] S. Boyd and L. Vandenberghe, *Convex Optimization*. Cambridge, UK: Cambridge University Press, 2004.
- [9] M. Azimi-Sadjadi, A. Pezeshki, L. Scharf, and M. Hohil, "Wideband doa estimation algorithms for multiple target detection and tracking using unattended acoustic sensors," in *Proc. of SPIE'04 Defense and Security Symposium, Unattended Ground Sensors IV*, vol. 5417, 2004.
- [10] M. Grant and S. Boyd, "CVX: Matlab software for disciplined convex programming, version 2.0 beta," <http://cvxr.com/cvx>, Sept. 2012.
- [11] B. Treeby and B. Cox, "k-Wave a Matlab toolbox for the time-domain simulation of acoustic wave fields," <http://www.k-wave.org>, Nov. 2012.